*J. Plasma Phys.* (2022), *vol*. 88, 175880501  
Published by Cambridge University Press

doi:10.1017/S0022377822000757

LETTER

# Seeking turbulence optimized configurations for the Wendelstein 7-X stellarator: ion temperature gradient and electron temperature gradient turbulence

**Sven Stroteich [1],†, Pavlos Xanthopoulos[2], Gabriel Plunk [2] and Ralf Schneider[1]**

[1]Institut für Physik, Universität Greifswald, 17489 Greifswald, Germany

[2]Max-Planck Institute for Plasma Physics, 17491 Greifswald, Germany

(Received 5 January 2022; revised 6 August 2022; accepted 8 August 2022)

We examine the turbulence driven by the ion and electron temperature gradients in selected magnetic configurations of the Wendelstein 7-X (W7-X) stellarator. The inherent flexibility in the configuration space of W7-X enables us to find candidate configurations manifesting low turbulent transport. We follow insights gained by stellarator optimization techniques, in order to identify key geometric features, which are directly related to the ion and electron heat fluxes produced by plasma turbulence. One such a feature is the flux expansion at locations where the curvature is particularly unfavourable. Starting from a configuration routinely used in the W7-X experiment, we end up with an optimized configuration. Based on this equilibrium, we select a configuration from W7-X configuration database with a similar feature as the optimized one. With the help of nonlinear gyrokinetic simulations, we show that the heat flux in this configuration is less stiff than in the initial configuration, both for ion temperature gradient and electron temperature gradient turbulence.

**Key words:** fusion plasma, plasma simulation, plasma instabilities

## 1. Introduction

Classical stellarators suffer historically from large neoclassical losses. Numerical stellarator optimization (Nührenberg & Zille 1986) was applied for the design of Wendelstein 7-X (W7-X) (Grieger *et al.* 1992) to overcome this problem. This success, however, leaves unsolved the problem of turbulent losses, underscoring the need for further optimization of the magnetic geometry. From previous studies (Xanthopoulos *et al.* 2014) one expects that the stellarator optimization, traditionally based on reduction of neoclassical fluxes by modifying Fourier components in the representation of the magnetic field, can be adapted for the reduction of turbulent transport. During the last campaign of

† Email address for correspondence: stroteichs@uni-greifswald.de

the W7-X experiment, it has been observed that for electron cyclotron resonance heated (ECRH) plasmas, the confinement time is similar to that predicted by the International Stellarator Scaling 2004 (ISS04) scaling law (Weller *et al.* 2009), and the ion temperature does not rise beyond an upper limit, of around 1.5 keV, independently of the input power. This feature has been attributed to the strong stiffness of the turbulence transport driven by the ion temperature gradient (ITG) (Beurskens *et al.* 2021).

Regarding electron heat transport in W7-X, although theoretical work has demonstrated that electron temperature gradient (ETG) turbulence should be relatively benign in plasmas with species of equal temperature (Plunk *et al.* 2019), recent experimental evidence shows that ETG turbulence can still be relevant in ECRH heated scenarios, where the electron temperature can greatly exceed the ion temperature (Weir *et al.* 2021). Such ECRH-heated plasmas are planned to be further investigated also in the upcoming experimental campaign for W7-X.

The optimization of magnetic configurations for stellarators with respect to the neoclassical transport (Mynick 2006) seems to still leave us with the necessary freedom to optimize the geometry of the magnetic field for improved turbulent transport, as demonstrated theoretically in recent works (Mynick, Pomphrey & Xanthopoulos 2010; Xanthopoulos *et al.* 2014). The present work takes a practical approach to exploring this possibility, within the configuration space of W7-X.

In the next section, we will describe how we obtained optimized configurations and what their characteristics are in terms of metric coefficients. Then, we will introduce our turbulence simulations set-up for ITG and ETG turbulence. We find that the magnetic configurations found through optimization demonstrate that a lower transport 'stiffness' is possible, as compared with the standard configurations: although these configurations do not have a very different 'critical gradient', corresponding to the threshold in the temperature gradient for the onset of finite turbulence, they do have a lower transport at a fixed gradient above the threshold. We henceforth use the terminology 'reduced stiffness' in the above sense.

## 2. Optimization

In this work we are interested in the optimization of turbulent transport. Therefore, we want to find favourable geometric configurations which give us a reduced stiffness. We argue that the key effect is the reduction of the effective gradient of the background temperature due to a modified flux expansion. The effect can be understood using the gyro-Bohm scaling of the heat flux for species $\alpha$ through the metric element $g^{xx}$ as

$$Q_{gB,\alpha} \propto \left(\frac{\rho_\alpha}{L_{T_\alpha,\mathrm{eff}}}\right)^2 = \rho_\alpha^2 \left(\frac{1}{L_{T_\alpha}}\right)^2 g^{xx}, \tag{2.1}$$

where $1/L_{T_\alpha,\mathrm{eff}} = \sqrt{g^{xx}}/L_{T_\alpha} = |\nabla \ln T_\alpha|$. Here, the radial coordinate is defined as $x = \sqrt{s}$, where $s$ is the normalized toroidal flux and $L_{T_\alpha}$, $L_{T_\alpha,\mathrm{eff}}$ are characteristic length scales of the temperature gradient. Physically, (2.1) shows how simply replacing the temperature scale length in the mixing-length estimate of transport can strongly effect the transport. To achieve the reduction of the stiffness, we exploit the effect of flux expansion by minimizing $\left|\nabla s^2\right| = (4s_0/a^2)g^{xx}(z=0)$, where $s$ is the normalized toroidal flux and $a$ is the minor radius, and the gradient is evaluated at the outboard midplane of the configurations. Here, the magnetic field curvature is particularly strong and the ITG and ETG modes are most likely to be destabilized. The optimization produces in our case configurations with minimized $\sqrt{g^{xx}}$. These configurations can then be realized in the W7-X experiment and the effect of the optimization can be evaluated experimentally. The temperature gradient

https://doi.org/10.1017/S0022377822000757 Published online by Cambridge University Press

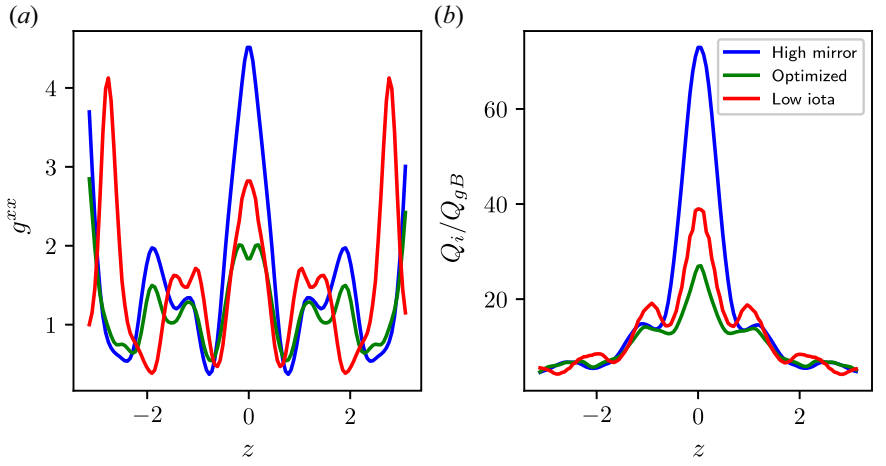


FIGURE 1. (*a*) Metric coefficient $g^{xx}$ and (*b*) ion heat flux produced by ITG turbulence, in gyro-Bohm units $Q_i/Q_{gB}$, as functions of the parallel coordinate $z$, using $a/L_{T_i} = 4.0$, for three different W7-X configurations: high-mirror configuration (blue), low-$\iota$ configuration (red) and optimized configuration (green).

is determined by metric and transport effects and is therefore not directly accessible experimentally.

Starting from the 'high-mirror' configuration, the optimization was achieved with the STELLOPT code (Spong *et al.* 2001) in fixed boundary mode. This set-up allows for more flexibility, with the downside that no information of coil currents is obtained, preventing direct application to experiment. To overcome this, we examined reference W7-X configurations to find a configuration with a similar feature as the optimized configuration. The target function for the optimization is $f = |g^{xx}|^2$ at $\theta = \phi = 0$ with the polodial and the toroidal Boozer angles, optimizing in the space of Garabedian coefficients $D_{m,n}$ with $|m| \leqslant 4$ and $|n| \leqslant 5$. All other Garabedian coefficients of the boundary were set to zero.

In figure 1(*a*) the results for the metric coefficient $g^{xx}$ as a function of the parallel coordinate $z$ are shown. Therefore, we study three different W7-X configurations, namely the high-mirror configuration, the optimized configuration and the low-$\iota$ configuration, which shows the smallest metric among the reference W7-X configurations. Here $\iota$ is the inverse of the safety factor $q$. As we see next, a quite substantial reduction of this quantity was achieved for the optimized configuration. The low-$\iota$ configuration shows also a clear reduction compared with the standard high-mirror configuration. In the following, we will show that this successful minimization results also in the reduction of ITG and ETG transport fluxes.

## 3. Turbulence simulations

To investigate the turbulent properties of the chosen magnetic configurations, we performed simulations using the gyrokinetic Vlasov code GENE (Jenko *et al.* 2000). This code solves the gyrokinetic equations simultaneously with Maxwell's equations, linearly or nonlinearly. We concentrate on the nonlinear simulations neglecting electromagnetic effects. Thus, we simulate a system with five dimensions where the gyromotion of the particles is eliminated by averaging over the Larmor orbit. The dimension are labelled as follows: $x$ denotes the radial coordinate, $y$ describes the binormal coordinate, $z$ is the parallel coordinate. Apart from the radial coordinate defined above, we have

https://doi.org/10.1017/S0022377822000757 Published online by Cambridge University Press

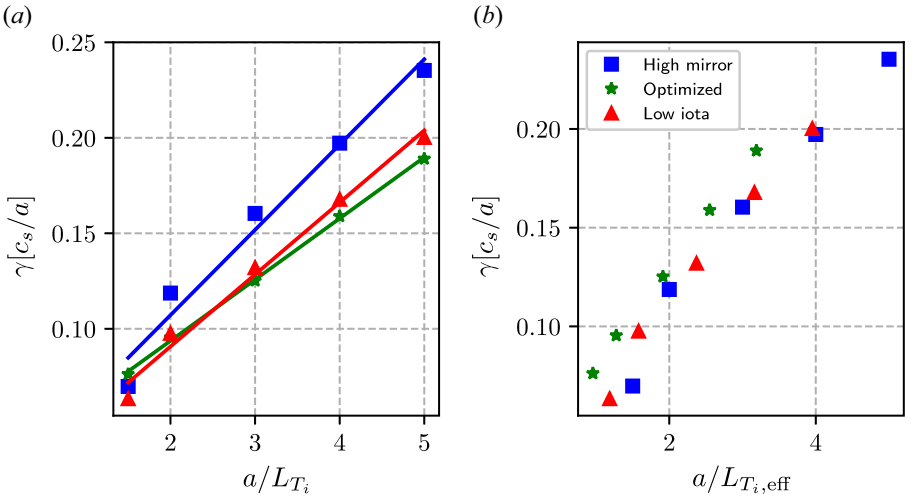


FIGURE 2. (*a*) Maximum linear growth rate produced by ITG turbulence, in units of $c_s/a$, as a function of the normalized ITG $a/L_{T_i}$. (*b*) Maximum linear growth rate produced by ITG turbulence, in units $c_s/a$, as a function of the normalized effective ITG $a/L_{T_i,\mathrm{eff}} = \sqrt{g^{xx}}/L_{T_i}$ for three different W7-X configurations: high-mirror configuration (blue squares), low-$\iota$ configuration (red triangles) and optimized configuration (green stars).

$y = s/q(q\theta - \phi)$ and $z = \theta$. Furthermore, $\mu$ is the magnetic moment, connected to the perpendicular velocity, and $v_\parallel$ is the parallel velocity. The main species for each turbulence type (ITG/ETG) is treated gyrokinetically, while the other one is assumed to have an adiabatic response. Collisions or electromagnetic effects are not considered here.

### 3.1. *Simulation set-up*

We simulate a 'flux tube' (Beer, Cowley & Hammett 1995), which is a computational box around a single field line on a selected surface, here $s/s_0 = 0.25$, where $s$ denotes the toroidal flux normalized by its value at the last closed flux surface. We employ the flux tube centred at the point $\theta = \phi = 0$, where $\varphi$ and $\vartheta$ are the toroidal and poloidal Boozer angles, respectively, centred at the outboard midplane at the bean cross-section.

For the ITG turbulence simulations, the selected box size is $L_x = L_y = 125.664$ for the radial and binormal directions, respectively. Here, we normalize with respect to the gyroradius $\rho_s = c_s/a$, where $c_s$ is the ion sound speed and $a$ is the minor radius. The parallel coordinate ranges from $-\pi$ to $\pi$. The parallel velocity domain reads $L_{v_\parallel} = 3$ in units of thermal velocity, and for the adiabatic invariant we have $L_\mu = 9$ in units of $T_i/B_0$. The numbers of grid points are $n_x = 96$, $n_y = 64$, $n_z = 117$, $n_{v_\parallel} = 96$, $n_\mu = 10$ for the ITG simulations.

For the ETG turbulence simulations, we have selected $L_x = 3$, $L_y = \pi$, $L_{v_\parallel} = 3$, $L_\mu = 9$ with $n_x = 96$, $n_y = 64$, $n_z = 117$, $n_{v_\parallel} = 30$, $n_\mu = 12$.

### 3.2. *The ITG turbulence*

Ion temperature gradient turbulence is found in the W7-X experiment (Carralero *et al.* 2021), and is responsible for strong turbulent heat fluxes, especially for scenarios involving ECRH power. First, we consider the linear simulations shown in figure 2(*a*). Here, the most unstable linear growth rates for each configuration are displayed over the normalized ITG $a/L_{T_i}$. We can observe that these linear calculations already indicate a lower stiffness for the optimized configuration and the low-$\iota$ configuration. Since only the case $k_x = 0$ is

https://doi.org/10.1017/S0022377822000757 Published online by Cambridge University Press

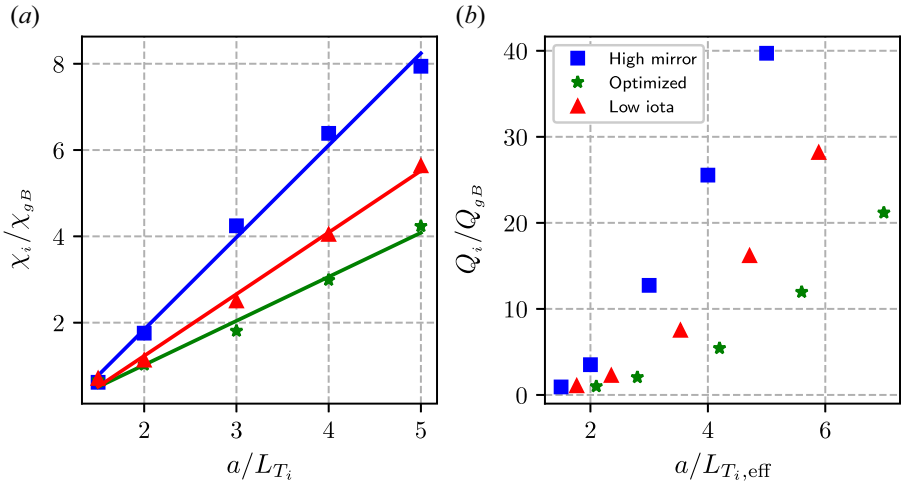


FIGURE 3. (*a*) Ion heat diffusivity produced by ITG turbulence, in gyro-Bohm units $\chi_i/\chi_{gB}$, as a function of the normalized ITG $a/L_{T_i}$. (*b*) Ion heat flux produced by ITG turbulence, in gyro-Bohm units $Q_i/Q_{gB}$, as a function of the normalized effective ITG $a/L_{T_i,\mathrm{eff}}$ for three different W7-X configurations: high-mirror configuration (blue squares), low-$\iota$ configuration (red triangles) and optimized configuration (green stars).

| Configuration | Stiffness [$\chi_{gB}$] |
|---|---|
| High mirror | 2.13 |
| Low $\iota$ | 1.43 |
| Optimized | 1.02 |

TABLE 1. Fitted stiffness for ITG turbulence in W7-X configurations.

studied here, the effect of the metric coefficient is not as prominent as expected. To get further evidence for the reduction, we will look at nonlinear simulations from now on. These are expanded along the radial direction, therefore, a larger distinction between the configurations is expected.

In figure 1, we show that the flux expansion, mathematically expressed through the metric component $g^{xx} = (a^2/4s_0)|\nabla s|^2$ correlates well with the calculated ion heat flux from ITG simulations. The maximum heat flux is located at the centre of the tube $z = 0$ for all configurations. More importantly, the configurations produce different maximum values of the heat flux according to the magnitude of their corresponding metric coefficient $g^{xx}$ at $z = 0$. The high-mirror configuration is characterized by a stronger heat flux compared with the optimized configuration and the low-$\iota$ configuration.

Analysing the dependence of the ion heat diffusivity, in gyro-Bohm units $\chi_i/\chi_{gB}$, with respect to the normalized ITG $a/L_{T_i} = -a/T_i\,\mathrm{d}T_i/\mathrm{d}r$, with $r = a\sqrt{s}$, we can compare the three configurations in figure 3. The difference in the resulting scaling is evident in the linear fits. The fit coefficients are listed in table 1. The slope parameter, quantifying ITG turbulence stiffness, is clearly reduced for the optimized configurations. Indeed, the low-$\iota$ configuration has a much smaller stiffness, by almost 33 %, compared with the high-mirror configuration. Not surprisingly, the reduction is even greater for the

https://doi.org/10.1017/S0022377822000757 Published online by Cambridge University Press

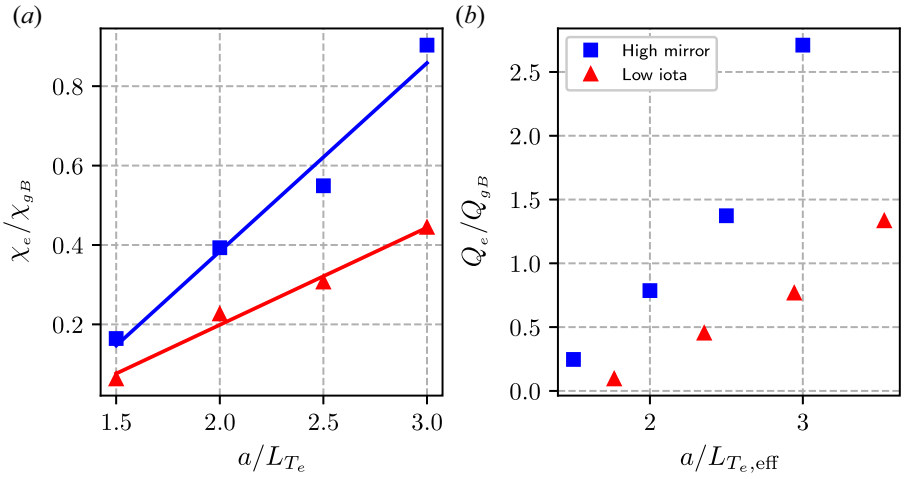


FIGURE 4. (*a*) Electron heat diffusivity produced by ETG turbulence, in gyro-Bohm units $\chi_e/\chi_{gB}$, as a function of the normalized electron temperature gradient $a/L_{T_e}$. (*b*) Electron heat flux produced by ETG turbulence, in gyro-Bohm units $Q_e/Q_{gB}$, as a function of the normalized effective electron temperature gradient $a/L_{T_e,\mathrm{eff}}$ for two different W7-X configurations: high-mirror configuration (blue squares) and low-$\iota$ configuration (red triangles).

| Configuration | Stiffness [$\chi_{gB}$] |
|---|---|
| High mirror | 0.47 |
| Low $\iota$ | 0.25 |

TABLE 2. Fitted stiffness for ETG turbulence in W7-X configurations.

optimized configuration, where the reduction is approximately 50 % compared with the initial configuration. On the other hand, the critical gradient does not vary significantly for the three configurations. Therefore, we conclude that minimizing ITG turbulence by the reduction of $g^{xx}$ reduces significantly the stiffness while not affecting the critical gradient.

### 3.3. *The ETG turbulence*

Electron temperature gradient turbulence is mostly important when considering ECRH scenarios since the electron temperature gradients become very large while the device is heated (Carralero *et al.* 2021). Therefore, we performed gyrokinetic simulations for ETG driven turbulence. Here, we excluded the optimized configuration since the calculation is much more resource intensive and the configuration cannot be achieved in the W7-X experiment, and thus is not as relevant for configuration studies for W7-X. Because the parallel variation of the electron heat flux behaves similarly to the ion heat flux, it is not shown here. The results of our scaling studies, similarly to those for ITG, are shown in figure 4. The low-$\iota$ configuration exhibits a much smaller stiffness than the high-mirror configuration. In table 2 one finds that ETG stiffness for the low-$\iota$ configuration is 50 % of the stiffness for the high-mirror configuration. These results support the expectation that the stellarator optimization done above reduces both ITG and ETG transport fluxes.

https://doi.org/10.1017/S0022377822000757 Published online by Cambridge University Press

## 4. Discussion

Next, we need to find an explanation for the large stiffness reduction for ETG and ITG for the low-$\iota$ configuration compared with the standard high-mirror configuration. A key turbulence saturation mechanism, that could provide an explanation, is zonal flows (Helander *et al.* 2011). These poloidally symmetric flows are typically present in ITG turbulence simulations, but not to the same degree in ETG turbulence simulations. To compare the zonal flow activity levels, a contour plot of the density and potential fluctuations for an ITG and an ETG simulation are shown in figure 5. The horizontal axis denotes the radial direction normalized by the gyroradius while the vertical axis denotes the binormal direction normalized by the gyroradius. In figure 5(*a*), the zonal flows are manifested as the broad structures along the binormal direction. In the ETG turbulence case, see figures 5(*b*) and 5(*d*), zonal flows are, as expected, absent. We can conclude that there is at least some reduction of stiffness by zonal flows for ITG turbulence. But the zonal flows do not play the major role for these three configurations since the stiffness reduction occurs for both ITG and ETG turbulence and is similar in size for both types of turbulence. Therefore, we assume that another mechanism must be responsible for the stiffness reduction.

As stated in (2.1) the major contribution of the reduction is connected to the minimization of $g^{xx}$. In figure 1 we emphasize the importance of the toroidal ITG and ETG modes that peak sharply in intensity at the location of strongest curvature, thus, only the value of $g^{xx}$ at $z = 0$ can be used rather than the flux-tube average of the metric coefficient to evaluate (2.1). To further illustrate the significance of flux surface expansion for the transport physics, we have provided three additional plots, figures 2(*b*), 3(*b*) and 4(*b*), following Angelino *et al.* (2009). By plotting the ion and electron heat fluxes versus effective gradients $a/L_{T,\mathrm{eff}}$, the transport levels can be observed to roughly 'collapse' to a single trend. Note that only the local measure of $g^{xx}(z = 0)$ is needed to interpret this behaviour, emphasizing the importance of the toroidal ITG and ETG modes that peak sharply in intensity at the location of strongest curvature.

For the interpretation of the results, in terms of confinement, we argue that a direct comparison of heat flux, at equal temperature gradients $a/L_T$, is appropriate. Generally, to interpret the heat flux, one can compute the total power crossing the flux surface. This can be written (see Helander *et al.* 2015) as

$$P = \hat{Q} Q_{gB} S(\rho), \tag{4.1}$$

where $S(\rho)$ is the surface area of the flux tube at the radial location $\rho$, $Q_{gB}$ is the gyro-Bohm value and $\hat{Q}$ is the heat flux density from our simulations. The corresponding values can be found in table 3. Taking a look at the last column, we see that the product of the scaling factors varies by only 5 % while the simulated heat flux is changing by 50 %. Thus, the description of the turbulent behaviour of the configurations can be understood via the simulated heat fluxes without additional modification factors.

## 5. Summary

We have identified a promising experimental W7-X configuration that shows reduced ITG and ETG transport stiffness compared with the standard high-mirror configuration. To achieve this, we used stellarator optimization, targeting the flux expansion factor. The low-$\iota$ configuration has an exceptionally small flux expansion at regions where the local curvature becomes strong, similar to the numerically optimized configuration. This explains the reduced turbulent heat flux compared with the high-mirror configuration. In particular, we find a reduction of the stiffness of 33 % for ITG and 50 % for ETG

https://doi.org/10.1017/S0022377822000757 Published online by Cambridge University Press

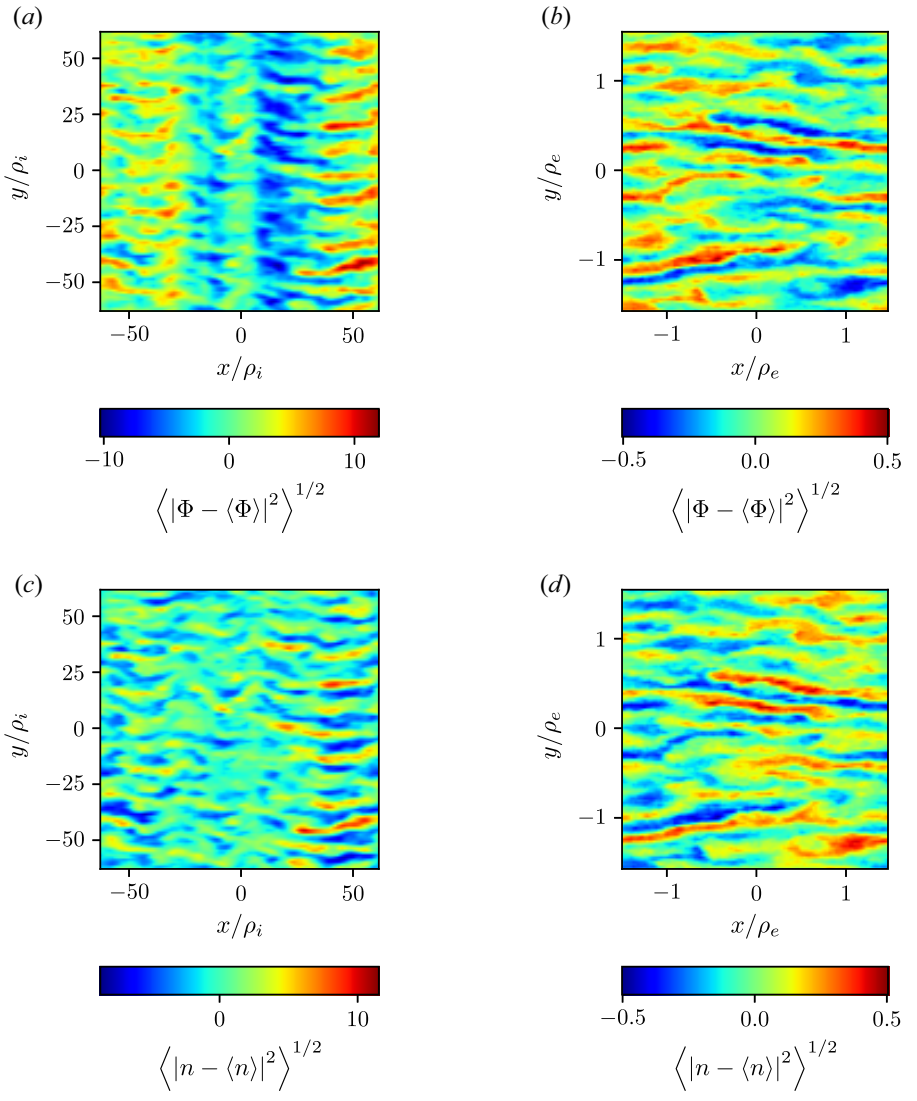


FIGURE 5. (*a*,*c*) Contours for the potential (up) and the density perturbations (down) from ITG turbulence simulation for the high-mirror configuration, using $a/L_{T_i} = 1.5$ at the outboard midplane at the bean cross-section. (*b*,*d*) Contours for the potential (up) and the density perturbations (down) from ETG turbulence simulation for the high-mirror configuration, using $a/L_{T_e} = 1.5$. For all cases, the horizontal axis ($x$) denotes the radial direction normalized by the gyroradius, and the vertical axis ($y$) denotes the binormal direction normalized by the gyroradius.

| Configuration | $Q_{gB}/Q_{gB_{\rm ini}}$ | $S/S_{\rm ini}$ | $Q_{gB}S/Q_{gB_{\rm ini}}S_{\rm ini}$ |
|---|---|---|---|
| High mirror | 1.00 | 1.00 | 1.00 |
| Low $\iota$ | 0.94 | 1.03 | 0.97 |
| Optimized | 0.90 | 1.06 | 0.95 |

TABLE 3. Coefficients to compare the heat flux in W7-X configurations.

https://doi.org/10.1017/S0022377822000757 Published online by Cambridge University Press

turbulence as characterized by the slopes of the heat flux plotted versus temperature gradient. We hope that the commissioning of the low-$\iota$ configuration will provide a better performance for the W7-X experiment in the next campaign, particularly alleviating the so-called '$T_i$-clamping' effect.

Finally, we wish to note that the simulation work in this paper has certain restrictions, most importantly the assumption that the density profile is flat. Although this assumption holds well in the core of an ECRH heated plasma, it cannot provide a good approximation for the neutral beam injection heating or pellet scenarios. In such cases, other micro-instabilities can also grow, such as the trapped electron mode (TEM) and the associated turbulence. Our next work is going to deal with the effect of optimization on TEM turbulence. This work is related to the maximum-$J$ property of the W7-X stellarator (Alcusón *et al.* 2020) since the second adiabatic invariant has an high influence on the trapped particles, but it is computationally rather expensive due to the inclusion of kinetic electrons.

## Acknowledgements

The GENE simulations have been performed on the RZG centre (Garching) and the Greifswald University Computer Centre.

*Editor William Dorland thanks the referees for their advice in evaluating this article.*

## Declaration of interests

The authors report no conflict of interest.

## REFERENCES

Alcusón, J.A., Xanthopoulos, P., Plunk, G.G., Helander, P., Wilms, F., Turkin, Y., von Stechow, A. & Grulke, O. 2020 Suppression of electrostatic micro-instabilities in maximum-$J$ stellarators. *Plasma Phys. Control. Fusion* **62** (3), 035005.

Angelino, P., Garbet, X., Villard, L., Bottino, A., Jolliet, S., Ghendrih, Ph., Grandgirard, V., McMillan, B.F., Sarazin, Y., Dif-Pradalier, G., *et al.* 2009 Role of plasma elongation on turbulent transport in magnetically confined plasmas. *Phys. Rev. Lett.* **102**, 195002.

Beer, M.A., Cowley, S.C. & Hammett, G.W. 1995 Field-aligned coordinates for nonlinear simulations of tokamak turbulence. *Phys. Plasmas* **2** (7), 2687–2700.

Beurskens, M.N.A., Bozhenkov, S.A., Ford, O., Xanthopoulos, P., Zocco, A., Turkin, Y., Alonso, A., Beidler, C., Calvo, I., Carralero, D., *et al.* 2021 Ion temperature clamping in Wendelstein 7-X electron cyclotron heated plasmas. *Nucl. Fusion* **61** (11), 116072.

Carralero, D., Estrada, T., Maragkoudakis, E., Windisch, T., Alonso, J.A., Beurskens, M., Bozhenkov, S., Calvo, I., Damm, H., Ford, O., *et al.* 2021 An experimental characterization of core turbulence regimes in Wendelstein 7-X. *Nucl. Fusion* **61** (9), 096015.

Grieger, G., Lotz, W., Merkel, P., Nührenberg, J., Sapper, J., Strumberger, E., Wobig, H., Burhenn, R., Erckmann, V., Gasparino, U., *et al.* 1992 Physics optimization of stellarators. *Phys. Fluids* B*: Plasma* **4** (7), 2081–2091.

Helander, P., Bird, T., Jenko, F., Kleiber, R., Plunk, G.G., Proll, J.H.E., Riemann, J. & Xanthopoulos, P. 2015 Advances in stellarator gyrokinetics. *Nucl. Fusion* **55** (5), 053030.

Helander, P., Mischchenko, A., Kleiber, R. & Xanthopoulos, P. 2011 Oscillations of zonal flows in stellarators. *Plasma Phys. Control. Fusion* **53** (5), 054006.

Jenko, F., Dorland, W., Kotschenreuther, M. & Rogers, B.N. 2000 Electron temperature gradient driven turbulence. *Phys. Plasmas* **7** (5), 1904–1910.

Mynick, H.E. 2006 Transport optimization in stellarators. *Phys. Plasmas* **13** (5), 058102.

MYNICK, H.E., POMPHREY, N. & XANTHOPOULOS, P. 2010 Optimizing stellarators for turbulent transport. *Phys. Rev. Lett*. **105**, 095004.

NÜHRENBERG, J. & ZILLE, R. 1986 Stable stellarators with medium $\beta$ and aspect ratio. *Phys. Lett.* A **114** (3), 129–132.

PLUNK, G.G., XANTHOPOULOS, P., WEIR, G.M., BOZHENKOV, S.A., DINKLAGE, A., FUCHERT, G., GEIGER, J., HIRSCH, M., HOEFEL, U., JAKUBOWSKI, M., *et al.* 2019 Stellarators resist turbulent transport on the electron larmor scale. *Nucl. Fusion* **122**, 035001.

SPONG, D.A., HIRSHMAN, S.P., BERRY, L.A., LYON, J.F., FOWLER, R.H., STRICKLER, D.J., COLE, M.J., NELSON, B.N., WILLIAMSON, D.E., WARE, A.S., *et al.* 2001 Physics issues of compact drift optimized stellarators. *Nucl. Fusion* **41** (6), 711–716.

WEIR, G.M., XANTHOPOULOS, P., HIRSCH, M., HÖFEL, U., STANGE, T., PABLANT, N., GRULKE, O., ÄKÄSLOMPOLO, S., ALCUSÓN, J., BOZHENKOV, S., *et al.* 2021 Heat pulse propagation and anomalous electron heat transport measurements on the optimized stellarator W7-X. *Nucl. Fusion* **61** (5), 056001.

WELLER, A., WATANABE, K.Y., SAKAKIBARA, S., DINKLAGE, A., FUNABA, H., GEIGER, J., HARRIS, J.H., OHDACHI, S., PREUSS, R., SUZUKI, Y., *et al.* 2009 International stellarator/heliotron database progress on high-beta confinement and operational boundaries. *Nucl. Fusion* **49**, 065016.

XANTHOPOULOS, P., MYNICK, H.E., HELANDER, P., TURKIN, Y., PLUNK, G.G., JENKO, F., GÖRLER, T., TOLD, D., BIRD, T. & PROLL, J.H.E. 2014 Controlling turbulence in present and future stellarators. *Phys. Rev. Lett*. **113**, 155001.